

Ash and gas discharge during open vent activity at El Reventador (Ecuador): explosion-style transitions driven by conduit capping

Freddy Vásconez, Yves Moussallam, Philipson Bani, Jean Battaglia, Silvana Hidalgo, Mhammed Benbakkar, Andrew Harris, Diego Narvaez

▶ **To cite this version:**

Freddy Vásconez, Yves Moussallam, Philipson Bani, Jean Battaglia, Silvana Hidalgo, et al.. Ash and gas discharge during open vent activity at El Reventador (Ecuador): explosion-style transitions driven by conduit capping. Bulletin of Volcanology, 2022, 84 (8), pp.77. 10.1007/s00445-022-01585-1 . hal-03874826

HAL Id: hal-03874826
https://hal.science/hal-03874826

Submitted on 28 Nov 2022

HAL is a multi-disciplinary open access archive for the deposit and dissemination of scientific research documents, whether they are published or not. The documents may come from teaching and research institutions in France or abroad, or from public or private research centers.

L'archive ouverte pluridisciplinaire **HAL**, est destinée au dépôt et à la diffusion de documents scientifiques de niveau recherche, publiés ou non, émanant des établissements d'enseignement et de recherche français ou étrangers, des laboratoires publics ou privés.



Distributed under a Creative Commons Attribution 4.0 International License

Ash and gas discharge during open vent activity at El Reventador (Ecuador): explosion-style transitions driven by conduit capping

Vásconez, F.[1,2], Moussallam, Y.[3], Bani, P[1]., Battaglia, J. [1] Hidalgo, S.[2], Mhammed Benbakkar[1], Harris, A.[1], Narváez, D.[4]

1- *Université Clermont Auvergne, CNRS, IRD, OPGC, Laboratoire Magmas et Volcans, F-63000 Clermont-Ferrand, France*
2- Instituto Geofísico, Escuela Politécnica Nacional, Ap. 17-01-2759, Quito, Ecuador
3- Lamont-Doherty Earth Observatory, Columbia University, New York, USA
4- Departamento de Geología, Escuela Politécnica Nacional, Ladrón de Guevara E11-253, Quito, Ecuador

Abstract

Since the VEI 4 eruption of November 2002, El Reventador volcano (Ecuador) has been the site of persistent open-vent activity characterized by frequent (hourly) Vulcanian – Strombolian explosions and occasional (every few years) effusion of lava flows. The conduit processes that sustain this continuous eruptive activity are still poorly understood. Here we combine high temporal resolution thermal infrared imaging with seismic recordings and DOAS-derived SO_2 fluxes focusing on a period of Vulcanian-style activity on 22-23 February 2017. Thermal imagery captured the emission and ascent dynamics of 26 plumes during the observation period, including those fed by explosions and degassing episodes. While most explosions have associated seismic signals, a few are marked by the absence of measurable seismic activity. Degassing episodes also show very few associated seismic signals. Explosions and degassing events seem to follow a sequence that can be explained by changes in the conduit permeability associated with rapid (over time scales of minutes) rheological stiffening of magma in the uppermost portion of the conduit to reduce degassing efficiency. Periods of open-vent outgassing alternate with periods of conduit capping resulting in system pressurization and leading to Vulcanian explosions that re-open the conduit allowing outgassing to resume.

Keywords:

Vulcanian explosion, Strombolian explosion, Ash Venting, Open vent, Ecuador

Resumen

Desde la erupción VEI 4 de noviembre de 2002, el volcán El Reventador (Ecuador) ha sido protagonista de una actividad persistente en sistema abierto (open-vent) caracterizada por explosiones Vulcanianas — Estrombolianas frecuentes (en el orden de horas), y efusión de flujos de lava y piroclásticos ocasionales (en el orden de meses a años). Los procesos en el conducto que sustentan esta continua actividad eruptiva son aún poco conocidos. En este trabajo combinamos el análisis de imagen térmica infrarroja en alta resolución temporal con análisis de señales sísmicas y flujo de SO_2 obtenido mediante DOAS, enfocándonos en el periodo de actividad tipo Vulcaniana ocurrida durante el 22 y 23 de febrero de 2017. Las imágenes térmicas registraron la dinámica de emisión y ascenso de 26 plumas durante el periodo de observación, incluyendo aquellas alimentadas por explosiones y episodios de desgasificación. Aunque la mayoría de las explosiones tienen señales sísmicas asociadas, unas pocas se caracterizan por la ausencia de actividad sísmica registrada en los sensores. Los periodos de desgasificación también presentan señales sísmicas asociadas muy pequeñas. Las explosiones y eventos de desgasificación parecen seguir una secuencia o ciclo que puede ser explicado por cambios en la permeabilidad del conducto asociados a una variación rápida (en la escala de minutos) de la rigidez del magma en la parte más somera del conducto, con lo que se limitaría la eficiencia de la desgasificación. La alternancia de periodos de desgasificación en conducto abierto con periodos de taponamiento del conducto da lugar a una presurización del sistema derivando en explosiones Vulcanianas que vuelven a abrir el conducto, lo que reanuda la secuencia con un nuevo proceso de desgasificación.

Introduction

Vulcanian eruptions involve short-lived intermittent explosive events that can continue for periods of years (Mercalli 1907). They are small to moderate in size, feeding eruptive columns typically reaching less than 10 km height, but which can collapse to generate pyroclastic flows (e.g., Marchetti et al. 2009; Yokoo 2009; Hall et al. 2015). Numerous recent volcanic eruptions have been catalogued as Vulcanian including at Sakurajima volcano in Japan since 1955 (Miwa and Toramaru 2013); Fuego volcano in Guatemala in 1978 (Wilson and Self 1980); Soufrière Hills volcano in Montserrat in 1997 (Formenti et al. 2003); Tungurahua volcano in Ecuador in 2013-2014 (Hidalgo et al. 2015; Hall et al. 2015; Battaglia et al. 2019; Gaunt et al. 2020); and El Reventador volcano in Ecuador since 2002 (Lees et al. 2008). Such Vulcanian eruptions can either be caused by phreatomagmatic or purely magmatic processes (cf. Clarke et al. 2015), but the classic model for magmatic Vulcanian eruptions is that they originate from the rupture of a gas-impermeable plug formed in the upper part of a magma-filled conduit (e.g., Fagents and Wilson 1993; Self et al. 1979; Sparks 1997; Woods 1995). Vulcanian eruptions are most commonly found at volcanoes erupting magmas of basaltic andesite to dacitic composition and usually emit only small amounts of ejecta (<1 km^3; Morrissey and Masting 1999). The velocity at which the material is expelled from the vent during Vulcanian explosions has been linked to the amount of gas involved in the event (Self et al. 1979; Wilson and Self 1980; Formenti et al. 2003; Clarke et al. 2015).

El Reventador volcano is a stratovolcano located on the rear-arc zone at the boundary of the Eastern cordillera and Amazon basin in Ecuador (Fig. 1a). Its currently active cone is located inside a horseshoe-shaped amphitheater that is 4 km wide (north-south) and 6 km long (northwest – southeast) and open to the southeast (Fig. 1b). Since 1541, this volcano has experienced more than 20 eruptive episodes (Siebert et al. 2011; Naranjo et al. 2016) of which seven occurred in the twentieth century (Hall et al. 2004). The first and the longest episode of the twentieth century took place from 1898 to 1912, and subsequent eruptive episodes had variable durations of up to 3 years, each separated by periods of around 12 years of quiescence. The last eruptive episode of the twentieth century ended in 1976. All of these eruptive episodes were “moderate” to “moderate-large” in scale (i.e., VEI 2-3), with Strombolian to Vulcanian eruptive styles (cf. Newhall and Self 1982), and produced blocky lava flows, small-volume pyroclastic and debris flows, and ash fallout (Hall et al. 2004; Samaniego

et al. 2008). El Reventador's most recent and still ongoing (at the time of writing) eruptive episode began in November 2002 with a VEI 4 explosion that destroyed the summit and crater of the cone, leaving deep notches on the northern and southern margins of the summit, and produced an eruptive column that rose up to 16-17 km above the crater (Hall et al. 2004). Pyroclastic flows were produced and reached the Coca river, ~9 km to the east of the active vent, destroying the main oil pipelines and the road leading to the oilfields of Ecuador. Ecuador's capital city, Quito, located ~100 km to the west (Fig. 1c), had to close down its international airport for eight days to allow ash clean-up operations that required removal of 1-2 mm ash produced by the intense ash fall of November 3 (Hall et al. 2004). During the first year after the paroxysmal event, two lava flows were emplaced from the summit and from a lateral vent in the southeastern cone flank (Samaniego et al. 2008; Naranjo et al. 2016). After around 1 year of quiescence, in 2004, new lava flows formed, followed by the alternation of effusive and mildly explosive periods (Lees et al. 2008; Ortiz et al. 2020). By 2015, the volcanic cone had a similar shape to that which existed before 2002 (Ortiz et al. 2020). Between 2016 and 2018, Almeida et al. (2019) documented a series of morphologic changes in the upper edifice, including the existence of two active vents in January 2016, a lateral eruption in June 2017, and a partial summit collapse in April 2018. By the time of our observations in February 2017, five effusive episodes had been identified by Naranjo et al. (2016) and Arnold et al. (2017). The discharge rate within each of the effusive periods was variable, with a general decreasing trend from one period to the next (Lees et al. 2008; Naranjo et al. 2016; Arnold et al. 2017). From 2012 through 2020, and continuing during effusive episodes, a variable number of explosions (up to 50 per day) were recorded by the local monitoring network operated by the Instituto Geofísico of Escuela Politécnica Nacional (IGEPN) (cf. Ramon et al. 2021). These transient explosions typically produced ash columns of variable ash content and height, ascending up to 2 km above the summit crater (e.g., Instituto Geofísico 2010, 2018, 2019). Similar activity has been observed at other open-vent andesitic through dacitic systems as, for example Sangay in Ecuador (Johnson and Lees 2000), Karymsky in Kamchatka (Johnson and Lees 2000) and Santiaguito in Guatemala (Johnson et al. 2008; Sahetapy-Engel et al. 2008; Sahetapy-Engel and Harris 2009). Models proposed to explain the generation of such explosions include accumulation of gas under a near-surface structure, i.e., a plug or a viscoelastic lava dome acting as pressure valve, that is released by the mechanical failure of the blocking structure (Johnson and Lees 2000; Johnson et al. 2008). A second model explains

ash eruptions at such open-vent system as being generated by slip events to cause shear-induced magma fragmentation at the conduit boundaries around the ascending dacite plug (Gonnermann and Manga 2003; Bluth and Rose 2004; Sahetapy-Engel et al. 2008).

Here, our aim is to analyze the ongoing volcanic activity at El Reventador to propose an explanation for the generation of the Vulcanian explosions and the associated plume dynamics. We present two-hours of quasi-continuous thermal video to describe the evolution of the activity, the duration of each explosion and propose a classification based on explosion characteristics. The flux of SO_2 emitted during the same period was measured by scanning DOAS (Differential Optical Absorption Spectroscopy; Platt and Stutz 2008) while the seismic activity was recorded by broadband seismometers at both proximal (~4 km) and distal (~45 km) locations (REVN and CAYA, Fig. 1c). Together, these observations suggest a sequence of four phases of activity reflecting evolving conditions in the shallow conduit. The sequence starts with no degassing and pressure build-up and is followed by destruction of a cap during a Vulcanian explosion. Thereafter, there is a phase of open-vent degassing punctuated by small Strombolian explosions as gas slugs episodically reach the surface. Afterwards, a new plug develops by cooling of the uppermost magma in the conduit, causing gas emissions to decrease until the system becomes fully plugged again; thereafter the cycle recommences.

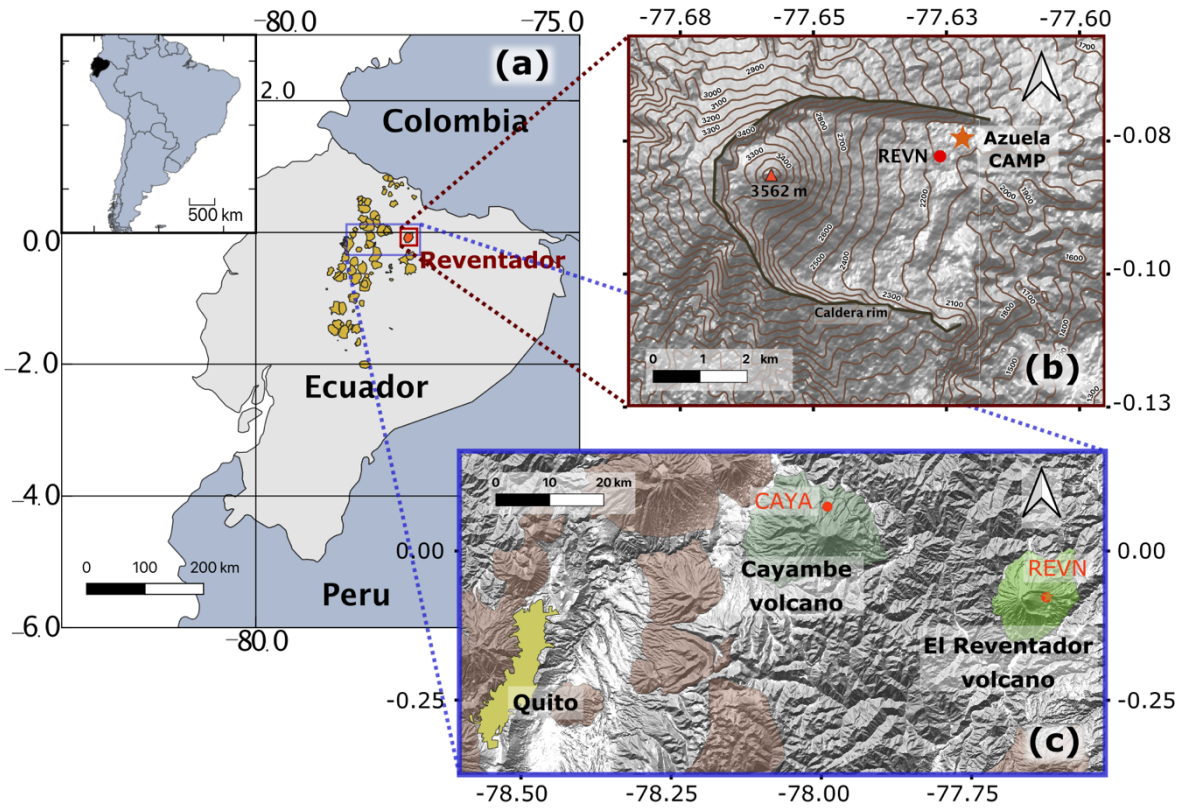


Fig. 1 (a) Location of El Reventador in Ecuador where yellow symbols are volcanoes active during the Holocene. Note that El Reventador is located to the east of the eastern side of the cordillera in Ecuador. (b) Enlargement on the current active cone at El Reventador, where “Azuela CAMP” is the site from which measurements were made and “REVN” is the proximal seismic station. (c) Map of the region to the West of El Reventador showing the location of the distal seismic station (“CAYA”), located in the northern flank of Cayambe volcano, and the city of Quito.

Methodology

The dataset analyzed here was acquired during a field campaign in February 2017 and consists of three types of recordings: (1) Thermal infrared video, (2) Scanning DOAS for SO_2 flux, and (3) Seismic. These we used together with visual observations and major element composition analysis of the emitted ash, which was simultaneously collected with the geophysical data sets (cf. Thivet et al. 2021).

Thermal analysis

Thermal videos were recorded from the Azuela CAMP site, located 4.5 km to the ENE of the active crater (latitude 0.07577S, longitude 77.62473W, altitude 2160 m a.s.l., Fig. 1b). We used an Optris PI 640 thermal infrared (8 – 14 μm) camera with a lens that produces a field of view of 15° × 11° and a 640 × 480 pixel image. The pixel size corresponding to a 4.5 km distance to the summit is 1.85 m. Videos of explosive events were captured at a rate of 32 frames per second (fps), with the thermal recording covering a quasi-continuous period of 2 hours, from 23h14 UTC on February 22 to 01h33 UTC on February 23.

To track and define thermal waveforms associated with the explosive events, a region of interest was defined directly above the crater rim (R1, Fig. 2) to capture any emission of hot fragments, ash and/or hot gases (Harris and Ripepe 2007a). A second region of interest (R2) was placed 1.85 or 3.7 m vertically above R1 (Fig. 2) to determine the ascent velocity from the delay in waveform onset between R1 and R2 (Sahetapy-Engel et al. 2008). Retrieving the kinetic temperature of fragments and hot gasses requires a correction for atmospheric absorption and emission, as well as emissivity effects (Harris 2013). Here, since we are interested in the relative changes of thermal signal instead of the absolute kinetic temperatures, and given minimal atmospheric effects at these altitudes (cf. Harris 2013), we present our data in terms of uncorrected brightness temperatures (cf. Matsushima 2005; Bani et al. 2013). The thermal amplitude is defined as the difference between the peak temperature and background temperature in any waveform (Harris and Thornber 1999; Ripepe et al. 2005). The timestamps for the time series were recorded using the operating computer, cross calibrated to GPS time.

Durations of ash and/or gas venting were also obtained from these thermal time series. In most cases, the starting and ending points of an explosion are clearly defined (Fig. 3). In some cases, however, when there is a phase of slow ash dispersal at the end of the event, the definition of the end of the explosion becomes ambiguous. In such a situation, we define the end of the event as the instant when the temperature inside the region R1 drops below the limit set as twice the background temperature (Fig. 3).

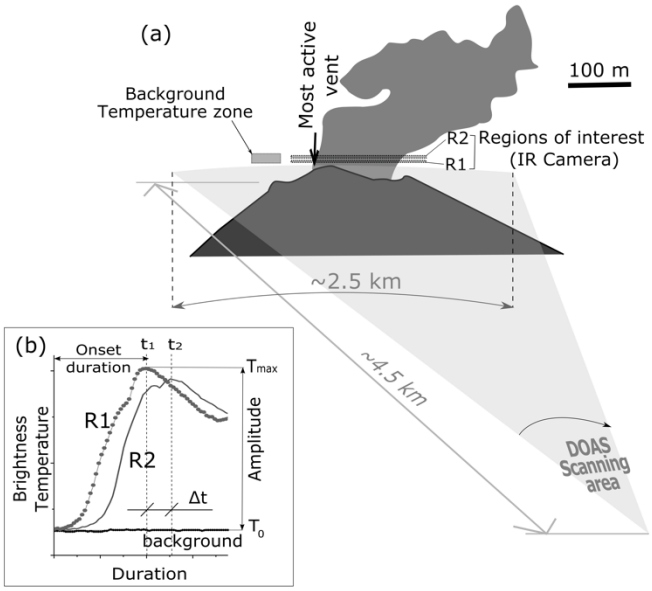


Fig. 2 (a) Layout of the measurement setup. The thermal camera and the DOAS were located 4.5 km to the east of the active cone. Two regions of interest (R1 and R2) are placed directly above the crater to track any fluctuation in the temperature due to hot material exiting the vent. The temperature of the background was also measured in the clear sky region as indicated. Also marked is the horizontal scanning plane covered by the DOAS. (b) Timeseries obtained from R1 and R2. Definition of the time delay between the peak temperature recorded at R1 (t_1) and R2 (t_2) as used to calculate ascent speed, onset time (the time to move from background temperature, T_0, to peak temperature, T_{max}), and thermal amplitude (T_{max}-T_0) (after Harris and Ripepe, 2007). Example is from the onset of explosion 4.

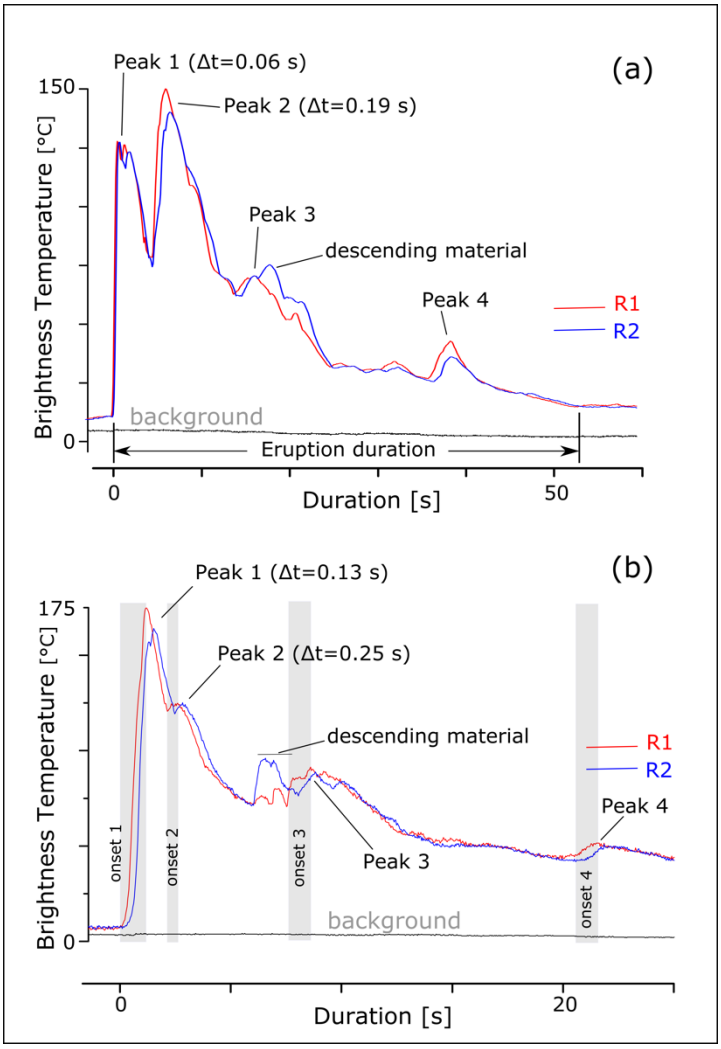


Fig. 3 Time series from regions of interest R1 (red line) and R2 (blue line) for explosions (a) *11* and (b) *13*. When hot pulses of ash and/or gas transit through R1 and R2, they trigger an impulsive increase in temperature, followed by a slower decrease. Objects first cross R1 and then R2, causing a delay between the two waveforms. Peaks that appear first in R2 before R1 correspond to hot bombs and blocks falling back to the ground. The time delay between a peak at R1 and its corresponding pike in R2 is signaled as Δt (Fig.2).

SO_2 flux

To estimate SO_2 flux we used a scanning DOAS from a fixed position at the Azuela CAMP site (Fig. 2). During measurements, the plume rose several hundred meters vertically above the summit before drifting to the east, enabling both horizontal and vertical scanning of the plume. Thirty-three spectra per scan were collected with a step angle of 0.9°, covering a horizontal scanned length of ~2.5 km in the horizontal configuration (Fig. 2a). The angular resolution was maintained when switching to the vertical configuration. The spectrometer

used was an Ocean Optics USB2000+ with a spectral range of 290-440 nm and a spectral resolution of 0.5 nm FWHM. The SO_2 column amounts (ppm.m) were retrieved using standard DOAS calibration and analysis procedures (Platt and Stutz 2008). Reference spectra included in the non-linear fit were obtained by convolving high resolution SO_2 (Bogumil et al. 2003) and O_3 (Voigt et al. 2001) cross sections with the instrument line shape. A Fraunhofer reference spectrum and Ring spectrum, calculated in DOASIS (DOAS Intelligent System; Kraus 2006), were also included in the fit. Measurements were made between 13h21 and 14h15, UTC, on February 23, 2017. The plume speed was calculated following the method described above in the paragraph of thermal analysis but also applied to periods of passive degassing. The plume transport speed relative error is conservatively assumed to be around 30–35%, which is towards the higher end of the range of past estimates (e.g., Arellano et al. 2008; Bani 2012; Bani et al. 2013b).

Seismicity

We used two broadband seismic stations from the permanent monitoring network of the IGEPN: REVN located 4 km from the summit of El Reventador and CAYA located 45 km to the west on the northern flank of Cayambe volcano (Fig. 1). Both stations are equipped with Trillium Compact 120s sensors with Q330 Kinemetrics digitizers. Data are recorded with a 100 Hz sampling frequency. Station REVN records both explosion quakes and tremors from El Reventador. Instead station CAYA, while normally used to monitor the activity at Cayambe volcano, also records the most energetic explosion-quakes from El Reventador.

Ash composition

Ash fall deposited during the observation period was collected and analyzed for major element bulk composition. To do this, 100 mg of sample was mixed with 300 mg of $LiBO_2$, melted in an induction oven at 1050 °C for 4.5 min using graphite crucibles. The resulting glass beads were then dissolved in a solution of deionized water and nitric acid (200 ml) and finally diluted by a factor of 2000. The solutions were analyzed by ICP-AES (An ULTIMA-C Horiba scientific, Jobin-Yvon spectrometer was used) at the Laboratoire Magmas et Volcans in Clermont-Ferrand (France).

Results

The activity we observed at El Reventador on 22 and 23 February 2017 was dominated by intermittent explosions that fed ash plumes up to about one kilometer above the summit, before detaching and being pushed to the east by the prevailing wind. The activity reports of IGEPN show a mean of 40 explosions per day and a similar number of long-period (LP) seismic events were recorded by station REVN. A small area of incandescent lava could be seen on the upper part of the northern flank of the cone. Most of the ejected blocks and bombs remained within the summit crater; although, during larger explosions, incandescent blocks were seen rolling down the flanks of the cone (Fig. 4).

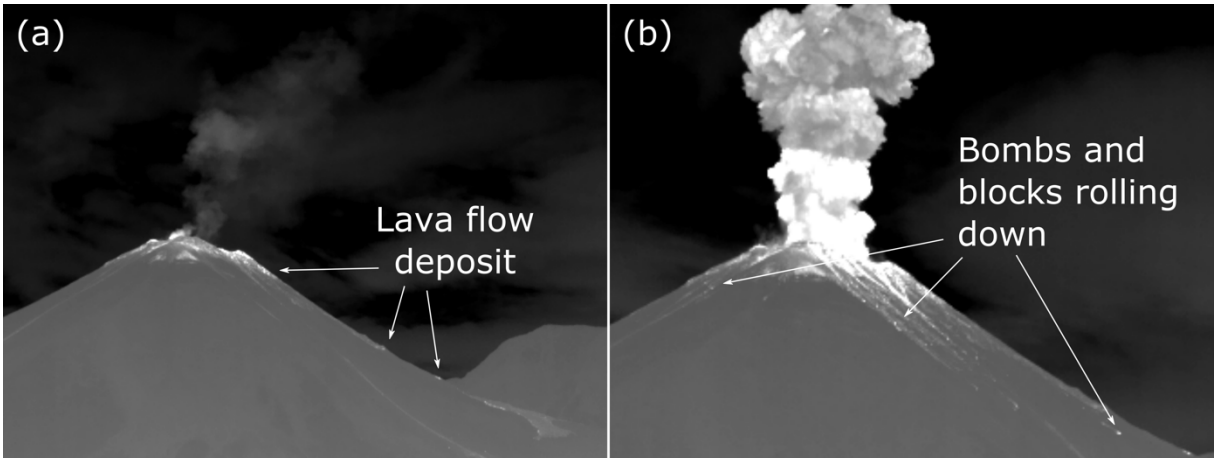


Fig. 4 Thermal infrared images of the summit area. (a) A small area of the deposit of a recent lava flow was recognizable on the northern flank. (b) During energetic explosions, most of the ejected blocks and bombs rolled down the flanks of the cone.

Thermal data

Thirteen explosions of variable thermal amplitude were recorded over the 2-hour measurement period. Another 13 less energetic degassing events were also recorded during this observation period. All thermal infrared videos are available in the Electronic Supplementary Material (ESM Video 01-Video 19).

Thermal amplitudes of the explosions varied between 40°C for the less energetic (minor) events (explosion 7) and up to 263 °C for the most energetic (major) events (explosion 3). Minor explosions only lasted for around 10 s, while major explosions persisted for up to 140 s. The 32 Hz acquisition rate of the thermal recording allowed a detailed thermal waveform to be generated for each event, highlighting successive thermal peaks within each explosive

discharge. Figure 5 shows an example of a sequence of thermal images acquired during an explosion with the corresponding thermal waveform. In this example, at least 11 thermal peaks are recorded over the 30 s of duration of the event highlighting a series of explosive pulses (cf. Harris et al. 2008). Generally, as in the Figure 5 waveform, the highest thermal amplitude recorded during any single explosion corresponded to the first or second peak, and amplitudes thereafter declined (cf. Fig. 3), consistent with a waning emission.

The time delay between consecutive peaks varies from 0.03 to up to 0.6 s, implying a decrease in velocity with increased delay (Fig. 2b). For our travel distance between R1 and R2 of 3.7 m, this gives velocity end members of 3 to 120 m s^{-1}, with an average of 27 m s^{-1}. We see from Figure 3 that the delay between any two peaks increases with time during any individual event, increasing from 0.06 to 0.19 s in Figure 3a and from 0.13 to 0.25 s in Figure 3b. This is consistent with a decrease in emission velocity with time, from 30 to 10 and 20 to 7 m s^{-1} in the two cases, respectively. The decay in thermal amplitude is also consistent with an event that decays in energy with time.

On the basis of thermal waveform (i.e., their thermal amplitude and duration), we classified the recorded emissions into three types (Fig. 6).

- Type A (Fig. 6a), is characterized by the highest thermal amplitudes (263 °C), longest durations (140 s) and highest plumes (> 800 m).
- Type B (Fig. 6b), is characterized by moderate thermal amplitudes (175 °C), durations of around 25 s and plume heights reaching up to 400 m.
- Type C (Fig. 6c) is characterized by the lowest thermal amplitudes (100 °C), durations of about 15 s and plume heights of up to 300 m.

This all implies a decrease in energy between each event type. We find that each event type tends to occur in a specific sequence (Fig. 7a). Type B and C events tend to occur together, with Type B punctuating clusters of repeated, at the rate of 0.2-0.7 Hz, Type C events (Fig. 7b) Such sequences are typically followed by explosion free periods (Fig. 7c), which are terminated by single, discrete Type A events (Fig. 7d). Explosion free periods show the existence of very low amplitude (10 °C) single peaked waveforms of 12 – 20 s in duration and which are associated with exhalations of gas (Fig. 7c). Within the sequence of Figure 7e, three individual

events of around 30 s in duration occurred with one minute delays, with decreasing thermal amplitudes.

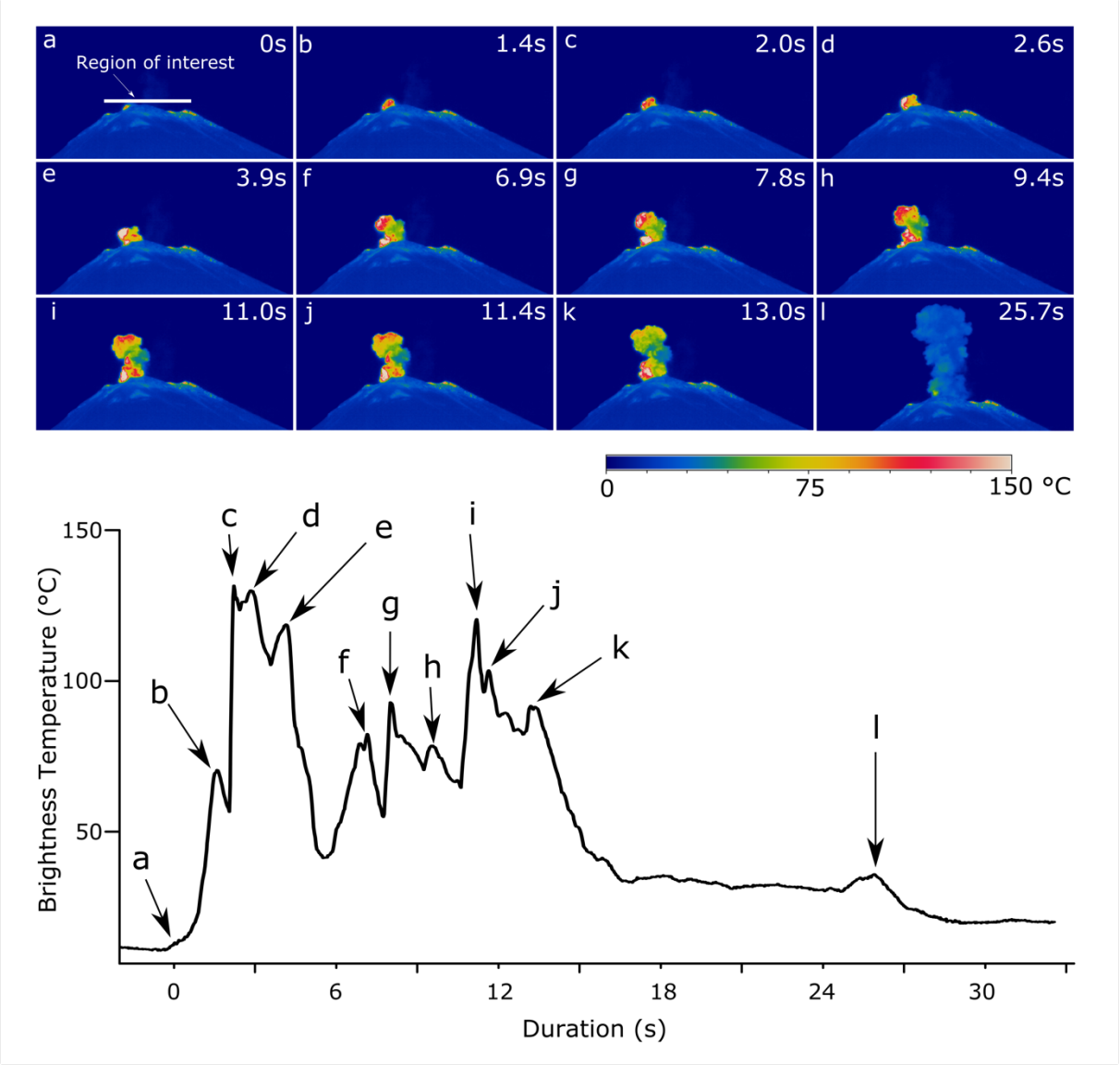


Fig. 5 Sequence of thermal images acquired during explosion *2* and the corresponding thermal waveform for the Region of Interest labelled in (a). Labelled letters on the waveform related to the location of thermal video frames (a) through (l). The eruption lasted 30s with 11 peaks each associated with a burst of material passing through the ROI (cf. Harris et al. 2008).

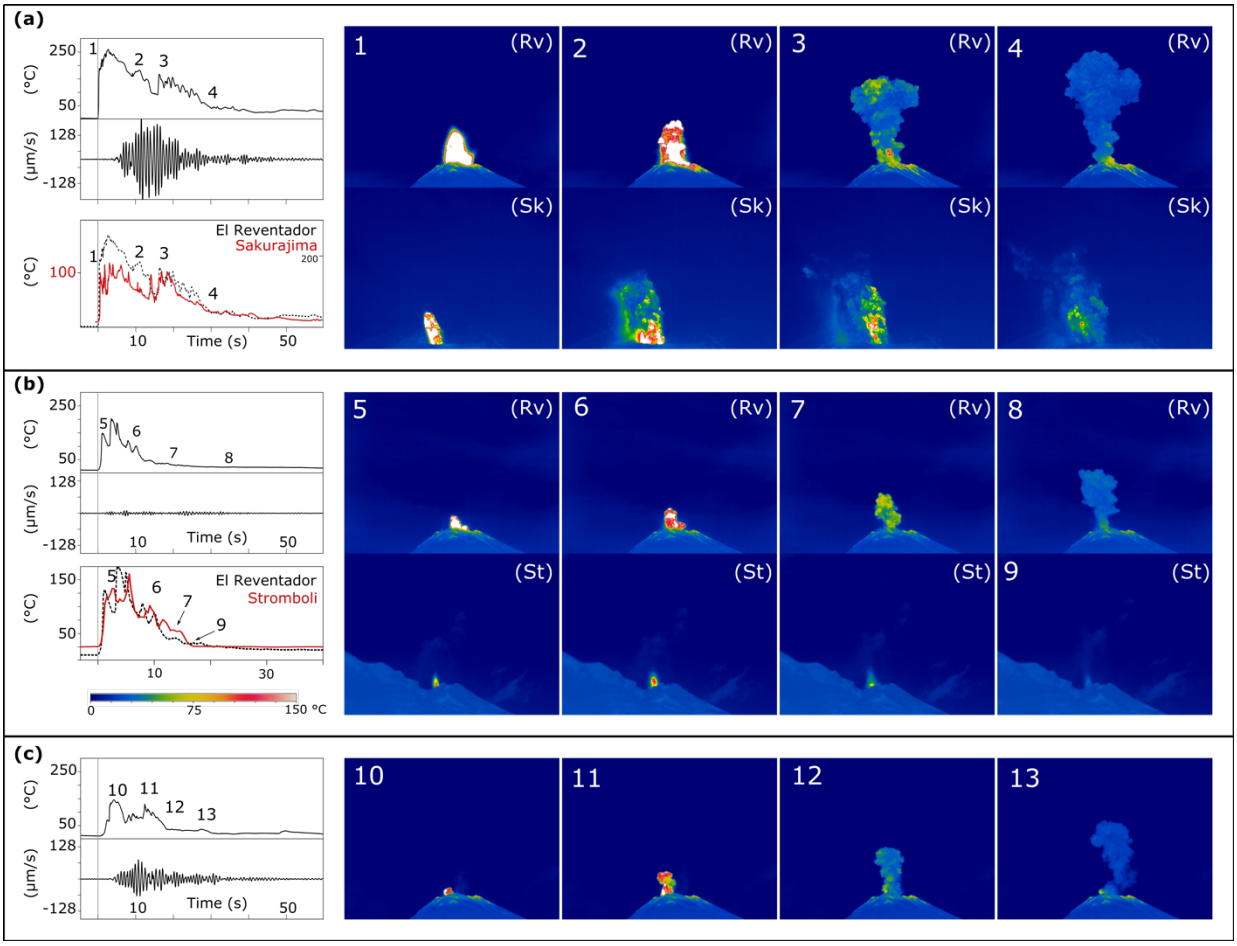


Fig. 6 Thermal and seismic waveforms for (a) Type A eruptions of Phase 4, (b) Type B eruptions of Phase 2, and (c) Type C eruptions of Phase 1. Thermal images in the right-hand panels correspond to the times shown as numbers (1-13). The thermal waveforms and duration of the Type A explosions in Phase 2 are similar to those of Sakurajima volcano (as plotted in red in a; data from A. Harris: Sakurajima eruption of 2013-07-27). The corresponding thermal images at Sakurajima, taken at similar time intervals as the Reventador ("Rv") are marked "Sk". In the case of Type A eruptions during Phase 4 (a), the thermal waveform and duration is comparable with those recorded at Stromboli volcano ("St") (as plotted in red in a; data from A. Harris: eruption at Stromboli recorded on 2008-06-03). The full videos with corresponding seismic and thermal waveforms from El Reventador can be found in the ESM.

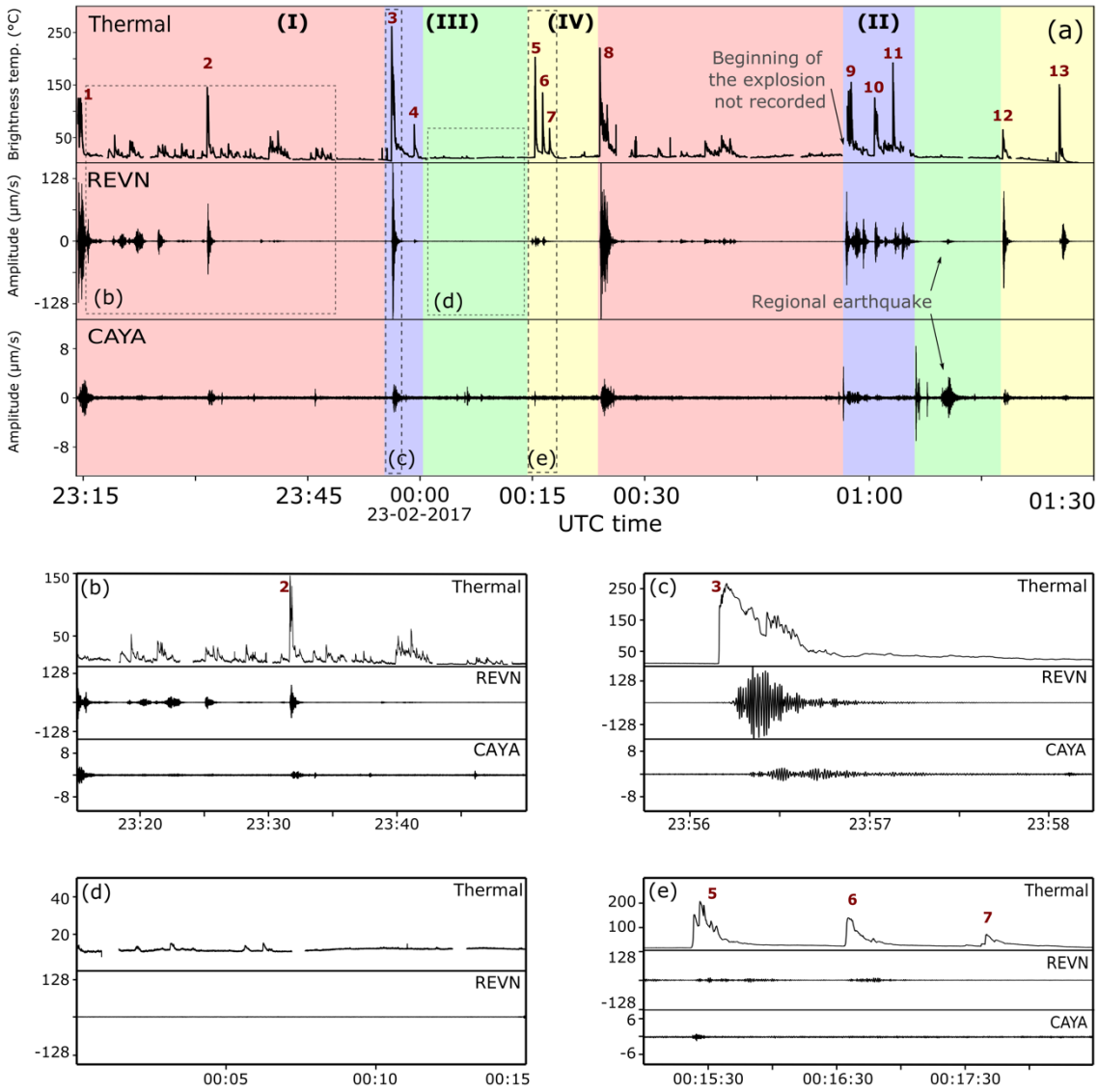


Fig. 7 (a)Temperature time series from region of interest R1 (Fig. 2) and the corresponding seismic signals from REVN and CAYA (Fig. 1). The main explosions are numbered from 1 to 13. Four distinct behavior, outlined with different background colors, can be distinguished from the thermal recording, including (b) a nearly continuous occurrence of Type B and C events, (c) Type A and B events (explosions 3, 9, 10, 11), (d) the low amplitude passive degassing phase; and (e) successive Type A and B event (explosions 5, 6, 7, 12, 13). Phases I, II, III, and IV occurred successively and repeated themselves once over the two hours recording, each sequence of phases lasting around one hour and 15 minutes.

SO_2 flux

Figure 8a shows the fluctuation of SO_2 column amount retrieved from the DOAS data. Sunrise was at about 06h30 (local time), even though light conditions at 08h00 were not optimal for DOAS measurements, there was sufficient light intensity to perform scanning considering that

our system has the capacity to modify automatically the integration time to allow acquisition of spectra with light intensity within an acceptable range. During our measurements, clouds started to develop progressively, first around and over the summit then directly above the scanner, as well as inside the caldera and between our observation site and the vent, forcing us at first to change the scanning orientation from horizontal to vertical, and finally to end the measurements. This also caused some periods of unreliable data (Fig. 8a). A mean plume velocity of 5.6 m s^{-1} was obtained using the thermal infrared camera video, allowing us to convert to SO_2 flux for approximately one hour of data as reported in Table 1. Fluxes fluctuated between 0.8 and 1.5 kg s^{-1} with a mean SO_2 emission rate of 1.1 ± 0.7 kg s^{-1} (Fig. 8b). The daily SO_2 emission rate from El Reventador was about 95 ± 60 tons per day during our observation.

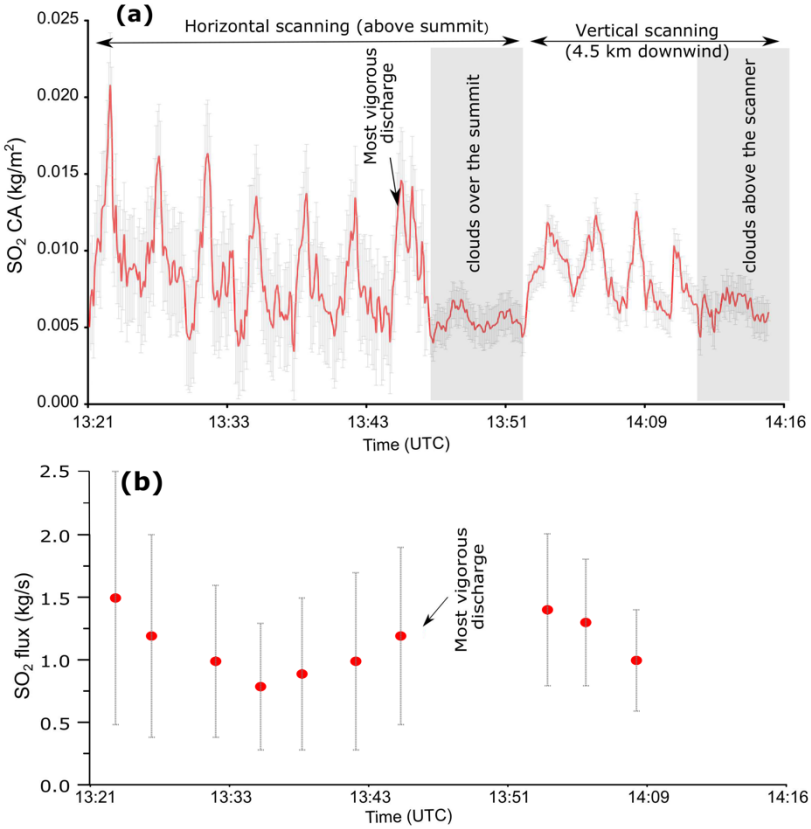


Fig. 8 (a) SO_2 column amount (CA) as derived from continuous scanning. The occurrence of clouds that triggered the shift from horizontal scanning to vertical scanning geometry, as well as the termination of scanning, is highlighted in gray. (b) The SO_2 flux calculated for each scan shows a cyclic trend despite the wide margin of errors.

Table 1. Results of SO_2 measurements performed on 23 February 2017 using scanning DOAS.

Scan	Start time (UTC)	End time (UTC)	Projected distance (m)	Number of spectra in the plume	Average column amount (g/m^2)	SO_2 flux (kg/s)
S1	13:21	13:24	1790	23	0.15	1.5 ± 1.0
S2	13:24	13:27	1400	18	0.14	1.2 ± 0.8
S3	13:31	13:33	1326	17	0.13	1.0 ± 0.6
S4	13:34	13:36	1170	15	0.12	0.8 ± 0.5
S5	13:38	13:41	1320	17	0.12	0.9 ± 0.6
S6	13:41	13:44	1560	20	0.11	1.0 ± 0.7
S7	13:44	13:47	1400	18	0.15	1.2 ± 0.7
S8	13:47	13:50		Clouds over the summit		
S9	13:50	13:52				
S10	14:02	14:04	552	24	0.35	1.4 ± 0.6
S11	14:05	14:07	276	12	0.35	1.3 ± 0.5
S12	14:07	14:10	460	20	0.32	1.0 ± 0.4
S13	14:10	14:12		Clouds above the scanner		
S14	14:12	14:15				
						Mean SO_2 flux estimation: 1.1 ± 0.7 kg/s

Seismicity

Using recordings from station REVN (Fig. 1), we identified nine signals that can be considered as explosion quakes, these are colored in blue in Figure 9. These explosion quakes are also clearly identified in the recordings of the station CAYA. Ten transient signals observed at CAYA are unrelated to the activity at El Reventador and are colored in red in Figure 9. These seismic signals correspond to volcano-tectonic events or ice quakes originating from Cayambe itself. In addition, three episodes of harmonic tremor were identified at REVN, colored green in Figure 9. Finally, both stations recorded a regional earthquake whose hypocenter was located in northern Peru by IGEPN (Fig. 7, Fig. 9).

The harmonic tremor episodes lasted a few minutes and always appeared after an explosion quake. All Type A events (explosions 5, 6, 7, 12 and 13) were recorded as low frequency

waveforms by the proximal seismic station (REVN) but not all of them appear in the distal (CAYA) seismic recordings (Fig. 9). Thermally, these explosions are associated with the highest energy events and have variable thermal amplitudes. However, theses amplitudes are not directly correlated to the amplitude of corresponding seismic signals.

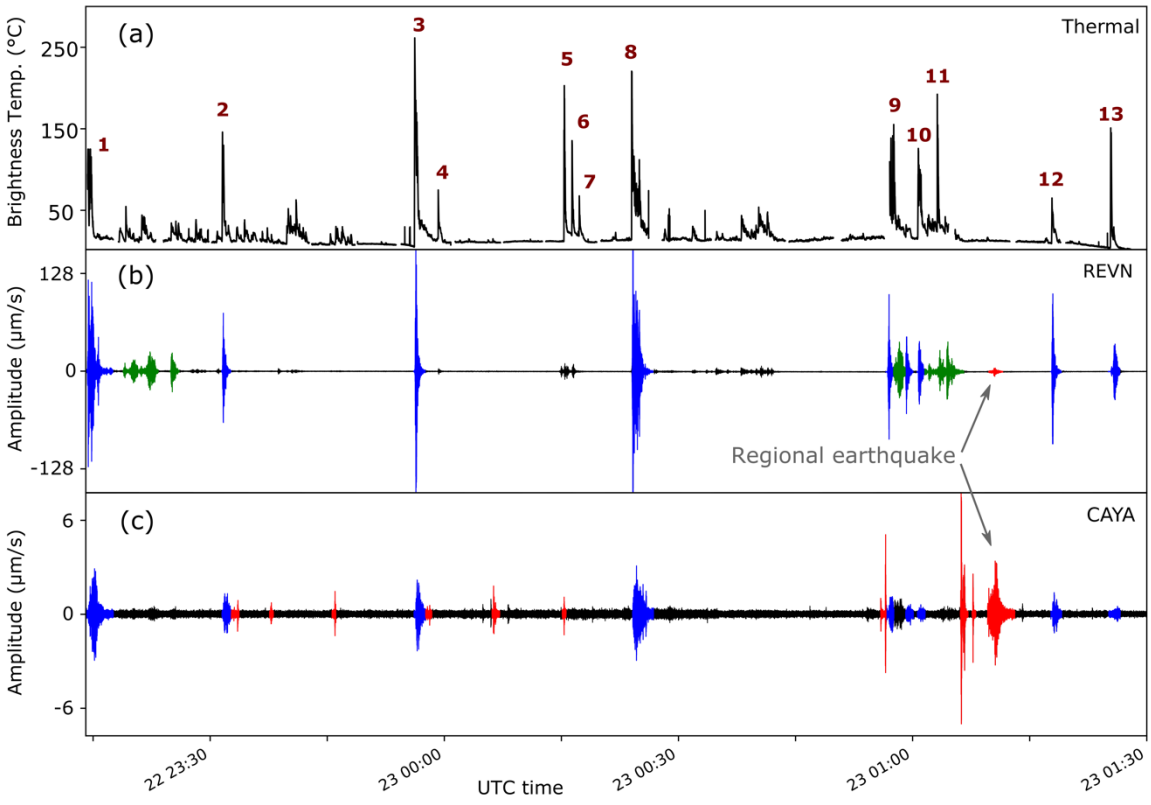


Fig. 9 (a) Timeseries of brightness temperature from thermal infrared imagery on which the thirteen Type A and B explosions are identified. (b) Seismic signals from station REVN, located 4 km to the east of the active crater. (c) Seismic signals from station CAYA, located 45 km to the northwest of El Reventador. Most of the explosions that can be identified at the proximal seismic station appear at the distal station as well (marked in blue). The seismic events colored in red are not related to El Reventador activity; they are volcano-tectonic events or ice quakes from Cayambe and a regional earthquake. Harmonic tremor episodes are highlighted in green; and are all preceded by an explosion. The sequence of explosions 5, 6 and 7 produced high thermal amplitudes but low seismicity. Instead, explosions 12 and 13 produced low thermal amplitudes but moderate seismic amplitudes.

Bulk Ash composition

The ash is of andesitic composition with SiO_2 contents around 58 wt. % (Table 2). The bulk ash composition falls in the trend displayed by whole rocks of El Reventador as reported by Samaniego et al. (2008) (Fig. 10).

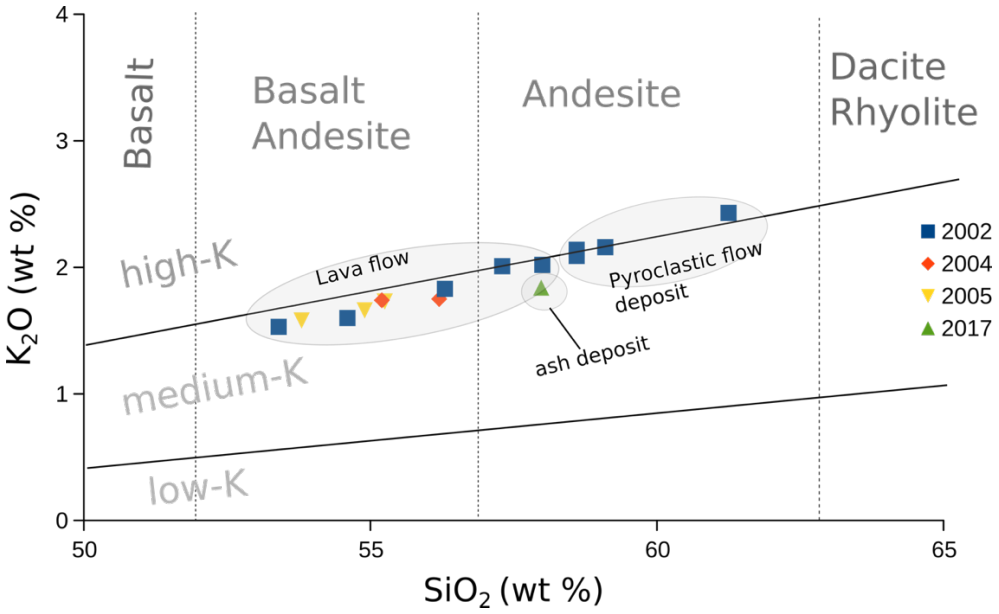


Fig. 10 K_2O versus SiO_2 classification diagram (Peccerillo and Taylor 1976) showing the composition of lavas extruded from El Reventador volcano between 2002 and 2005 (Samaniego et al. 2008) and the ash sample collected during our observation period.

Table 2. Bulk composition of ash samples collected following a Vulcanian explosion at El Reventador on 22 February 2017.

SiO_2 (wt%)	Al_2O_3 (wt%)	Fe_2O_3 (wt%)	MgO (wt%)	CaO (wt%)	Na_2O (wt%)	K_2O (wt%)	TiO_2 (wt%)	MnO (wt%)	P_2O_5 (wt%)	Ba (wt%)	Sr (wt%)	Total	H_2O (wt%)
57.98	17.67	6.93	3.76	6.73	3.57	1.84	0.88	0.11	0.37	0.14	0.10	100.08	0.24

Discussion

Based on coupled patterns in the thermal and seismic waveforms, as well as trends in the SO_2 flux time series, we can group our data into four successive phases (Fig. 7a). We emphasize that the dynamics presented in this work is representative of our period of observation and must then be extrapolated with caution, but we believe it gives a useful guide to the dynamics driving El Reventador's open-vent persistent explosive activity.

Phase 1 consists of about 30 minutes of quasi-continuous, minor bursts of gas and ash as seen in the thermal time series as a series of Type C and B events (Fig. 7a; ESM Video 03). These events appear with variable amplitudes in the proximal seismic station but are barely recorded by the distal seismic station (Fig. 7b).

Phase 2 consists of a single or series of Type A and B explosion(s) that last around two minutes (Fig. 7d; ESM Video 07). These events are clearly distinct from explosions seen in phase 1 as they expel an appreciable quantity of ballistics covering the upper part of the edifice and occasionally generate minor rock falls and pyroclastic density currents (cf. ESM Video 07 and ESM Video 03). Seismicity with high amplitude mirrors the high thermal amplitude signal (Fig. 7d). The duration, the waveform and thermal amplitude of the explosions occurring in this phase (Fig. 6a) are similar to those of ash venting occurring at Santiaguito volcano (Johnson et al. 2004; Sahetapy-Engel et al. 2008; Marchetti et al. 2009) and Vulcanian explosions at Sakurajima volcano (Yokoo 2009). Figure 6b shows the comparison between a Type A explosion of Phase 2 at El Reventador and one of Sakurajima's Vulcanian explosion recorded in July 2013 (A. Harris, unpublished data), where the duration and shape of the waveform are similar. We thus interpret these event types to be similar in terms of source, emission and ascent dynamics. We thereby label them "Vulcanian" and assume they are related to stick-slip of a highly viscous plug as at Santiaguito (cf. Bluth and Rose 2004; Sahetapy-Engel et al. 2008) or, more likely, failure of a high viscosity cap in the true Vulcanian sense (Johnson and Lees 2000; Hall et al. 2015)

Phase 3 consists of 10 to 15 minutes of passive degassing (Fig. 7c; ESM Videos 08 and 09). During this phase no explosions are recorded, either in the thermal or seismic records (n.b., signals registered at the CAYA station are not associated with El Reventador).

Finally, phase 4 consists of a period of about 10 minutes in which we record a series of Type B explosions (Fig. 7d; ESM Videos 10, 18 and 19). The seismic amplitude of these events is very small when compared to the seismic amplitude associated with the explosions recorded in phases 1 and 2 (Fig. 6) and is the only case where seismic and thermal signals are decoupled. The waveform of the thermal signal and the duration of the individual explosions in this phase (Fig. 6) are comparable to those observed in explosions at Stromboli (e.g. Harris and Ripepe

2007a; Harris et al. 2012; Patrick et al. 2005) and Villarrica (Marchetti et al. 2009), as shown in Figure 6c. We thus interpret these event types to be similar in terms of source, emission and ascent dynamics. We thereby label them “Strombolian” and assume they are related to bubble bursting at a relatively low viscosity surface (Shinohara 2005; Patrick et al. 2007) or at-least one that is thinly capped (Gurioli et al. 2014).

Activity developed through these four phases twice during the two-hour observation period. Although the SO_2 flux measurements could not be obtained concurrently (DOAS measurements rely on good sunlight while thermal measurements are best performed at night), they also oscillate over a timescale of about one hour thus following the same timescale of trend observed in the thermal and seismic recordings by visual observations.

Phase 1 characteristics can be interpreted as a conduit which is mostly plugged, or in the process of plug development. Degassing occurs as short bursts of “ash venting” associated with thermal and seismic signals and decreases over time, potentially indicating progressive sealing of the system. Ash venting may be the result of stick-slip events impacting the developing plug (cf. Neuberg 2000; Lensky et al. 2008). Such process can lead to a decrease in the permeability of the upper part of the conduit and, subsequently, to an increase in the pressurization of the system. The progressive decrease of the SO_2 flux, as evidenced in this work, further supports this observation. Phase 1 would hence correspond to the formation of a gas-impermeable cap in the upper part of the conduit (Del Bello et al. 2015; Capponi et al. 2016), probably caused by cooling and degassing of the shallowest portion of the magma column, which induces a rheological stiffening and increases magma viscosity (Gurioli et al. 2014). The energetic Type A explosion(s) characterizing phase 2 (Fig. 6a), can be interpreted as the culmination of pressure accumulation in the conduit, an accumulation which is finally released by one or a series of energetic explosions (Fig. 7a) destroying the cap. This model is consistent with the ejection of ballistics, the high amplitudes in both the thermal and seismic signals and the similarity with waveforms recorded during “Vulcanian” events at other systems (cf. Fig. 6). During phase 3, which is explosion-free, unhindered degassing occurs, and is interpreted as a period of purely open vent (uncapped) activity. Finally, in phase 4, with the system still in an open-vent configuration, gas slugs can travel through the upper part of the conduit and burst at the free surface producing intermittent “Strombolian” explosions. The

thermal amplitude of some of these explosions is not mirrored by the seismic amplitude, possibly because of a source at a shallower level than those with appreciable seismic amplitude at both proximal and distal stations (Fig. 7e). Our thermal, seismic and, to a lesser extent, SO_2 flux observations therefore highlight cyclic transitions at El Reventador between plugged and open vent configurations (Fig. 11).

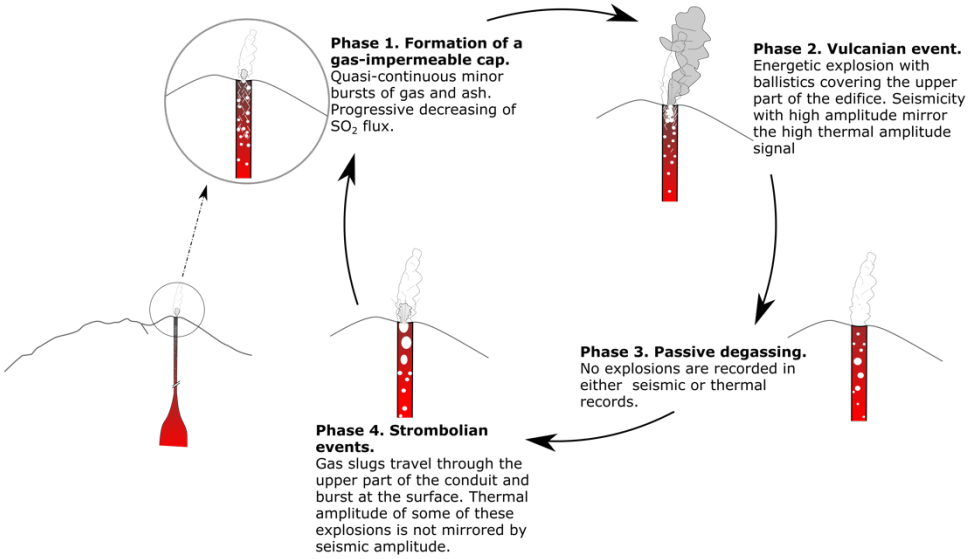


Fig. 11 In this work, the dynamics of El Reventador's activity can be characterised by 4 distinct phases: the formation of a gas-impermeable cap, the phase of Vulcanian explosions, a period of passive degassing and a phase of Strombolian explosions. This last phase gradually fades away as the permeability in the vent decreases and the impermeable cap starts to form.

Conclusion

Our analysis of thermal, seismic, and SO_2 flux measurements at El Reventador clearly highlights the temporal succession of different types of explosive and degassing activity that can be classified into four phases. Phase 1 is characterized by frequent, nearly continuous, explosions of small thermal and seismic amplitude diminishing with time, indicating the progressive self-sealing of the conduit. This restricts the gas flow and builds up pressure in the conduit. Phase 2 is characterized by one or several large explosions, associated with high thermal and seismic amplitudes and durations, indicating the destruction of the impermeable cap created during phase 1. Phase 3 is characterized by passive, unhindered degassing indicating entirely open vent conditions while phase 4 sees the episodic bursting of presumably isolated gas slugs at the surface. The entire sequence is repeated twice in a two-

hour observation period suggesting a cyclic oscillation between plugged and open vent configurations at El Reventador. The similarity with thermal and seismic waveforms from other classic Strombolian and Vulcanian (VEI 2 through 4) systems suggests the operation of common and globally applicable degassing and explosive processes that cause caps to develop and decay, thereby driving changes in eruption style.

Acknowledgements

Fieldwork for this research was conducted as part of the "Trail By Fire" expedition (PI: Y.M.) supported by the Royal Geographical Society (with the Institute of British Geographers) through the Land Rover Bursary; the Deep Carbon Observatory DECADE Initiative; Ocean Optics; Crowcon; Air Liquide; Thermo Fisher Scientific; Cactus Outdoor; Turbo Ace and Team Black Sheep. F.V. acknowledges support from the Region Auvergne Rhone Alpes through its call for projects Pack Ambition Recherche 2018 (project OROVOLC, PI: Y.M.). We thank IGEPN for kindly providing seismic data for this study. This research has been conducted in the context of the Laboratoire Mixte International "Séismes et Volcans dans les Andes du Nord" of IRD. We also thank Sylvie Vergniolle, the Associate Editor, and the anonymous reviewers for their constructive comments that improved this paper.

Bibliography

Almeida M, Gaunt H, Ramón P (2019) Ecuador's El Reventador Volcano Continually Remakes Itself. Eos 100:. https://doi.org/10.1029/2019EO117105

Arellano SR, Hall M, Samaniego P, et al (2008) Degassing patterns of Tungurahua volcano (Ecuador) during the 1999–2006 eruptive period, inferred from remote spectroscopic measurements of SO2 emissions. J Volcanol Geotherm Res 176:151–162. https://doi.org/10.1016/j.jvolgeores.2008.07.007

Arnold DWD, Biggs J, Anderson K, et al (2017) Decaying Lava Extrusion Rate at El Reventador Volcano, Ecuador, Measured Using High-Resolution Satellite Radar: DECAYING LAVA EXTRUSION AT EL REVENTADOR. J Geophys Res Solid Earth 122:9966–9988. https://doi.org/10.1002/2017JB014580

Bani P (2012) First estimate of volcanic SO2 budget for Vanuatu island arc. J Volcanol Geotherm Res 11

Bani P, Harris AJL, Shinohara H, Donnadieu F (2013a) Magma dynamics feeding Yasur's

explosive activity observed using thermal infrared remote sensing: YASUR THERMAL SENSING. Geophys Res Lett 40:3830–3835. https://doi.org/10.1002/grl.50722

Bani P, Surono, Hendrasto M, et al (2013b) Sulfur dioxide emissions from Papandayan and Bromo, two Indonesian volcanoes. Nat Hazards Earth Syst Sci 13:2399–2407. https://doi.org/10.5194/nhess-13-2399-2013

Battaglia J, Hidalgo S, Bernard B, et al (2019) Autopsy of an eruptive phase of Tungurahua volcano (Ecuador) through coupling of seismo-acoustic and SO2 recordings with ash characteristics. Earth Planet Sci Lett 511:223–232. https://doi.org/10.1016/j.epsl.2019.01.042

Bluth GJS, Rose WI (2004) Observations of eruptive activity at Santiaguito volcano, Guatemala. J Volcanol Geotherm Res 136:297–302. https://doi.org/10.1016/j.jvolgeores.2004.06.001

Bogumil K, Orphal J, Homann T, et al (2003) Measurements of molecular absorption spectra with the SCIAMACHY pre-flight model: instrument characterization and reference data for atmospheric remote-sensing in the 230–2380 nm region. J Photochem Photobiol Chem 157:167–184. https://doi.org/10.1016/S1010-6030(03)00062-5

Capponi A, James MR, Lane SJ (2016) Gas slug ascent in a stratified magma: Implications of flow organisation and instability for Strombolian eruption dynamics. Earth Planet Sci Lett 435:159–170. https://doi.org/10.1016/j.epsl.2015.12.028

Clarke AB, Esposti Ongaro T, Belousov A (2015) Vulcanian Eruptions. In: The Encyclopedia of Volcanoes. Elsevier, pp 505–518

Del Bello E, Lane SJ, James MR, et al (2015) Viscous plugging can enhance and modulate explosivity of strombolian eruptions. Earth Planet Sci Lett 423:210–218. https://doi.org/10.1016/j.epsl.2015.04.034

Fagents SA, Wilson L (1993) Explosive volcanic eruptions-VII. The ranges of pyroclasts ejected in transient volcanic explosions. Geophys J Int 113:359–370. https://doi.org/10.1111/j.1365-246X.1993.tb00892.x

Formenti Y, Druitt TH, Kelfoun K (2003) Characterisation of the 1997 Vulcanian explosions of Soufrière Hills Volcano, Montserrat, by video analysis. Bull Volcanol 65:587–605. https://doi.org/10.1007/s00445-003-0288-8

Gaunt HE, Burgisser A, Mothes PA, et al (2020) Triggering of the powerful 14 July 2013 Vulcanian explosion at Tungurahua Volcano, Ecuador. J Volcanol Geotherm Res 392:106762. https://doi.org/10.1016/j.jvolgeores.2019.106762

Gonnermann HM, Manga M (2003) Explosive volcanism may not be an inevitable consequence of magma fragmentation. Nature 426:432–435. https://doi.org/10.1038/nature02138

Gurioli L, Colo' L, Bollasina AJ, et al (2014) Dynamics of Strombolian explosions: Inferences from field and laboratory studies of erupted bombs from Stromboli volcano: DYNAMICS OF STROMBOLIAN EXPLOSIONS. J Geophys Res Solid Earth 119:319–345. https://doi.org/10.1002/2013JB010355

Hall M, Ramón P, Mothes P, et al (2004) Volcanic eruptions with little warning: the case of Volcán Reventador's Surprise November 3, 2002 Eruption, Ecuador. Rev Geológica Chile 31:349–358. https://doi.org/10.4067/S0716-02082004000200010

Hall ML, Steele AL, Bernard B, et al (2015) Sequential plug formation, disintegration by Vulcanian explosions, and the generation of granular Pyroclastic Density Currents at Tungurahua volcano (2013–2014), Ecuador. J Volcanol Geotherm Res 306:90–103. https://doi.org/10.1016/j.jvolgeores.2015.09.009

Harris A (2013) Thermal Remote Sensing of Active Volcanoes: A User's Manual. Cambridge University Press

Harris A, Ripepe M (2007a) Synergy of multiple geophysical approaches to unravel explosive eruption conduit and source dynamics – A case study from Stromboli. Geochemistry 67:1–35. https://doi.org/10.1016/j.chemer.2007.01.003

Harris A, Ripepe M (2007b) Temperature and dynamics of degassing at Stromboli. J Geophys Res 112:B03205. https://doi.org/10.1029/2006JB004393

Harris AJL, Ripepe M, Calvari S, et al (2008) The 5 April 2003 Explosion of Stromboli: Timing of Eruption Dynamics Using Thermal Data. In: The Stromboli Volcano: An Integrated Study of the 2002–2003 Eruption. American Geophysical Union (AGU), pp 305–316

Harris AJL, Ripepe M, Hughes EA (2012) Detailed analysis of particle launch velocities, size distributions and gas densities during normal explosions at Stromboli. J Volcanol Geotherm Res 231–232:109–131. https://doi.org/10.1016/j.jvolgeores.2012.02.012

Harris AJL, Thornber CR (1999) Complex effusive events at K¯ılauea as documented by the GOES satellite and remote video cameras. Bull Volcanol 61:14

Hidalgo S, Battaglia J, Arellano S, et al (2015) SO2 degassing at Tungurahua volcano (Ecuador) between 2007 and 2013: Transition from continuous to episodic activity. J Volcanol Geotherm Res 298:1–14. https://doi.org/10.1016/j.jvolgeores.2015.03.022

Instituto Geofísico EPN (2010) Informe de la actividad del volcán El Reventador durante el año 2009. Instituto Geofísico de la Escuela Politécnica Nacional

Instituto Geofísico EPN (2018) Informe Especial N°2 del volcán El Reventador – 2018. Instituto Geofísico de la Escuela Politécnica Nacional

Instituto Geofísico EPN (2019) Informe anual del volcán El Reventador – 2018. Instituto

Geofísico de la Escuela Politécnica Nacional
Johnson JB, Harris AJL, Sahetapy-Engel STM, et al (2004) Explosion dynamics of pyroclastic eruptions at Santiaguito Volcano: DYNAMICS OF SANTIAGUITO PYROCLASTIC ERUPTIONS. Geophys Res Lett 31:n/a-n/a. https://doi.org/10.1029/2003GL019079
Johnson JB, Lees JM (2000) Plugs and chugs—seismic and acoustic observations of degassing explosions at Karymsky, Russia and Sangay, Ecuador. J Volcanol Geotherm Res 101:67–82. https://doi.org/10.1016/S0377-0273(00)00164-5
Johnson JB, Lees JM, Gerst A, et al (2008) Long-period earthquakes and co-eruptive dome inflation seen with particle image velocimetry. Nature 456:377–381. https://doi.org/10.1038/nature07429
Kraus S (2006) DOASIS a framework design for DOAS. PhD Thesis, Technische Informatik, Univ.\ Mannheim
Lees JM, Johnson JB, Ruiz M, et al (2008) Reventador Volcano 2005: Eruptive activity inferred from seismo-acoustic observation. J Volcanol Geotherm Res 176:179–190. https://doi.org/10.1016/j.jvolgeores.2007.10.006
Lensky NG, Sparks RSJ, Navon O, Lyakhovsky V (2008) Cyclic activity at Soufrière Hills Volcano, Montserrat: degassing-induced pressurization and stick-slip extrusion. Geol Soc Lond Spec Publ 307:169–188. https://doi.org/10.1144/SP307.10
Marchetti E, Ripepe M, Harris AJL, Delle Donne D (2009) Tracing the differences between Vulcanian and Strombolian explosions using infrasonic and thermal radiation energy. Earth Planet Sci Lett 279:273–281. https://doi.org/10.1016/j.epsl.2009.01.004
Matsushima N (2005) H2O emission rate by the volcanic plume during the 2000-2002 Miyakejima volcanic activity: 2000-2002 MIYAKEJIMA VOLCANIC ACTIVITY. Geophys Res Lett 32:n/a-n/a. https://doi.org/10.1029/2005GL023217
Mercalli G (1907) Vulcani attivi della terra: morfologia–dinamismo–prodotti–distribuzione geografica–cause...
Miwa T, Toramaru A (2013) Conduit process in vulcanian eruptions at Sakurajima volcano, Japan: Inference from comparison of volcanic ash with pressure wave and seismic data. Bull Volcanol 75:685. https://doi.org/10.1007/s00445-012-0685-y
Morrissey M, Masting L (1999) Vulcanian eruptions. In: Encyclopedia of Volcanoes, 1st edn. San Diego, California, USA, pp 463–475
Naranjo MF, Ebmeier SK, Vallejo S, et al (2016) Mapping and measuring lava volumes from 2002 to 2009 at El Reventador Volcano, Ecuador, from field measurements and satellite remote sensing. J Appl Volcanol 5:8. https://doi.org/10.1186/s13617-016-0048-z

610 Neuberg J (2000) Characteristics and causes of shallow seismicity in andesite volcanoes. Philos
611 Trans R Soc Lond Ser Math Phys Eng Sci 358:1533–1546.
612 https://doi.org/10.1098/rsta.2000.0602
613 Newhall CG, Self S (1982) The volcanic explosivity index (VEI) an estimate of explosive
614 magnitude for historical volcanism. J Geophys Res 87:1231.
615 https://doi.org/10.1029/JC087iC02p01231
616 Ortiz HD, Matoza RS, Garapaty C, et al (2020) Multi-year regional infrasound detection of
617 Tungurahua, El Reventador, and Sangay volcanoes in Ecuador from 2006 to 2013. Acoustics
618 Virtually Everywhere, p 022003
619 Patrick MR, Hams A, Jonathan Dehn Luke Flynn William Gersch Robert Wright C (2005)
620 Strombolian Eruption Dynamics From Thermal (FLIR) Video Imagery
621 Patrick MR, Harris AJL, Ripepe M, et al (2007) Strombolian explosive styles and source
622 conditions: insights from thermal (FLIR) video. Bull Volcanol 69:769–784.
623 https://doi.org/10.1007/s00445-006-0107-0
624 Peccerillo A, Taylor SR (1976) Geochemistry of eocene calc-alkaline volcanic rocks from the
625 Kastamonu area, Northern Turkey. Contrib Mineral Petrol 58:63–81.
626 https://doi.org/10.1007/BF00384745
627 Platt U, Stutz J (2008) Differential optical absorption spectroscopy: principles and applications ;
628 with 55 tables. Springer, Berlin
629 Ramon P, Vallejo S, Mothes P, et al (2021) Instituto Geofísico – Escuela Politécnica Nacional,
630 the Ecuadorian Seismology and Volcanology Service. Volcanica 4:93–112.
631 https://doi.org/10.30909/vol.04.S1.93112
632 Ripepe M, Harris AJL, Marchetti E (2005) Coupled thermal oscillations in explosive activity
633 at different craters of Stromboli volcano: COUPLED THERMAL OSCILLATIONS AT
634 DIFFERENT CRATERS. Geophys Res Lett 32:. https://doi.org/10.1029/2005GL022711
635 Sahetapy-Engel ST, Harris AJL (2009) Thermal-image-derived dynamics of vertical ash
636 plumes at Santiaguito volcano, Guatemala. Bull Volcanol 71:827–830.
637 https://doi.org/10.1007/s00445-009-0284-8
638 Sahetapy-Engel ST, Harris AJL, Marchetti E (2008) Thermal, seismic and infrasound
639 observations of persistent explosive activity and conduit dynamics at Santiaguito lava dome,
640 Guatemala. J Volcanol Geotherm Res 173:1–14.
641 https://doi.org/10.1016/j.jvolgeores.2007.11.026
642 Samaniego P, Eissen J-P, Le Pennec J-L, et al (2008) Pre-eruptive physical conditions of El
643 Reventador volcano (Ecuador) inferred from the petrology of the 2002 and 2004–05 eruptions.

644 J Volcanol Geotherm Res 176:82–93. https://doi.org/10.1016/j.jvolgeores.2008.03.004
645 Self S, Wilson L, Nairn IA (1979) Vulcanian eruption mechanisms. Nature 277:440–443.
646 https://doi.org/10.1038/277440a0
647 Shinohara H (2005) Volcanic gases emitted during mild Strombolian activity of Villarrica
648 volcano, Chile. Geophys Res Lett 32:L20308. https://doi.org/10.1029/2005GL024131
649 Siebert L, Simkin T, Kimberly P (2011) Volcanoes of the World: Third Edition. University of
650 California Press
651 Sparks RSJ (1997) Causes and consequences of pressurisation in lava dome eruptions. Earth
652 Planet Sci Lett 150:177–189. https://doi.org/10.1016/S0012-821X(97)00109-X
653 Thivet S, Harris AJL, Gurioli L, et al (2021) Multi-Parametric Field Experiment Links
654 Explosive Activity and Persistent Degassing at Stromboli. Front Earth Sci 9:669661.
655 https://doi.org/10.3389/feart.2021.669661
656 Voigt S, Orphal J, Bogumil K, Burrows JP (2001) The temperature dependence (203–293 K)
657 of the absorption cross sections of O3 in the 230–850 nm region measured by Fourier-transform
658 spectroscopy. J Photochem Photobiol Chem 143:1–9. https://doi.org/10.1016/S1010-
659 6030(01)00480-4
660 Wilson L, Self S (1980) Volcanic explosion clouds: Density, temperature, and particle content
661 estimates from cloud motion. J Geophys Res 85:2567.
662 https://doi.org/10.1029/JB085iB05p02567
663 Woods AW (1995) A model of vulcanian explosions. Nucl Eng Des 155:345–357.
664 https://doi.org/10.1016/0029-5493(94)00881-X
665 Yokoo A (2009) Continuous thermal monitoring of the 2008 eruptions at Showa crater of
666 Sakurajima volcano, Japan. Earth Planets Space 61:1345–1350.
667 https://doi.org/10.1186/BF03352987
668